Spectrum of very excited Σ_g^+ flux tubes in SU(3) gauge theory

P. Bicudo,[*] N. Cardoso,[†] and A. Sharifian[‡]

CeFEMA, Departamento de Física, Instituto Superior Técnico (Universidade Técnica de Lisboa), Avenida Rovisco Pais, 1049-001 Lisboa, Portugal

(Received 28 May 2021; accepted 31 August 2021; published 28 September 2021)

Spectra with full towers of levels are expected due to the quantization of the string vibrations; however, different theoretical models exist for the excitation spectra. First principle computations are important to test the different models and to search for novel phenomena, but so far, only a few excited states of QCD flux tubes have been studied with pure gauge SU(3) lattice QCD in $3+1$ dimensions. We thus aim to study a spectrum of flux tubes with static quark and antiquark sources up to a significant number of excitations. We specialize on the spectrum of the most symmetric case, namely Σ_g^+, where up to two levels are already published in the literature. To achieve the highest possible excitation level, we construct a large set of operators with the correct symmetry, solve the generalized eigenvalue problem, and compare the results of different lattice QCD gauge actions with different lattice spacings and anisotropies.

DOI: 10.1103/PhysRevD.104.054512

I. INTRODUCTION

Understanding the confinement of color remains a main theoretical problem of modern physics. Its solution could also open the door to other unsolved theoretical problems. An important evidence of confinement, where we may search for relevant details to understand it, is in the QCD flux tubes [1], computed in lattice QCD. Experimentally, flux tubes are suggested by the Regge trajectories [2,3] in the hadron spectrum. String models can account for Regge trajectories, and they also imply the linear confining quark-antiquark potential similar to the one used in quark models [4,5].

Presently, an approximate understanding of flux tubes is quite developed, for example, with string models. The dominant behavior of the stringlike flux tubes has a single scale: the string tension σ. The main analytical string model utilized in the literature to explain the behavior of the QCD flux tubes is the Nambu-Goto bosonic [6,7] string model [8]. It assumes infinitely thin strings, with transverse quantum fluctuations only. The quantum fluctuations predict not only a finite profile width of the ground-state flux tube, increasing with distance [9], but also an infinite tower of quantum excitations [10,11]. However, the stringlike behavior obscures the details of confinement and of other possible hadronic phenomena.

Clearly, at short quark-antiquark distances, the flux tube deviates from the string model. The Nambu-Goto model in four space-time dimensions has an imaginary tachyon [11] at short distances for the ground state, whereas the QCD flux tube has a real Coulomb potential [11]. At really short distances, lattice QCD has recently shown the potential becomes dominated by perturbative QCD [12].

Another instance where the ground-state flux tube deviates from the string model is in the flux tube profile. Recently, our lattice QCD collaboration PtQCD [13] studied the zero temperature ground-state flux tube of pure gauge QCD and found evidence for a penetration length λ [14] as a second scale other than the string tension σ, contributing to the color fields density profile of the flux tube. This intrinsic width of the flux tube may be the reason why the QCD flux tube is stable in four dimensions, unlike the Nambu-Goto string, which is rotational invariant only in 26 dimensions.

There is also an ongoing puzzle in the excited spectrum of mesons, as reported [15] in measurements by the Cristal Barrel detectors [16]: The Regge slope for radial excitations is similar to the one for angular excitations, and this cannot be explained with a quark model [2]. A large degeneracy, larger than the chiral restoration symmetry [17], has been analyzed [18–21]. Possibly, there is a new principal quantum number [3]. Notice a principal quantum number is already present in the Nambu-Goto spectrum.

Besides, an infinite tower [22] of these excitations can also be obtained with constituent gluon models, in the denominated hybrid three body quark-gluon-antiquark systems [23,24]. This may possibly be explained by [3]

[*]bicudo@tecnico.ulisboa.pt
[†]nuno.cardoso@tecnico.ulisboa.pt
[‡]alireza.sharifian@tecnico.ulisboa.pt

a constituent gluon with an effective mass [25,26] and an effective quark gluon-gluon potential [27,28].

Moreover, there is evidence for another particle, the string worldsheet axion [29], in the lattice gauge theory spectra of closed strings.

Thus, precise first principle theoretical studies are necessary to go beyond the string models and clarify the details of QCD flux tubes or hybrid. In lattice QCD, it is straightforward to study ground-state open flux tubes, using the technique of Wilson loops [1], the simplest gauge invariant correlations in lattice QCD.

There are two classes of flux tubes: the closed flux tubes and the open ones. In lattice QCD, they are, respectively, studied with torelons and Wilson loops. There has been a serious effort of extracting higher excitations in the closed flux tube channel [30,31]. The spectrum of the closed flux tube can be partially approximated by the Nambu-Goto model.

In this paper, we study the excited open flux tubes in lattice QCD. In particular, we opt to address the puzzling sector of radial excitations. Some excited states have indeed been observed by lattice QCD computations [32–38], so far compatible with the string dominance of the QCD flux tube. Moreover, the structure of excited flux tubes started to be studied as well [39–41], where some evidence for a constituent gluon is present in some states. However, only the first excitations have so far been studied.

The spectrum of radial excitations of the ground state is the Σ_g^+ spectrum. We now review the symmetry group of our flux tubes. With two static sources, it is equivalent to the one of the molecular orbitals of homonuclear diatomic molecules. It is the point group denominated $D_{\infty h}$. We thus utilize the standard quantum number notation of molecular physics, already adopted in the previous studies of QCD flux tube excitations [32–38,40,41]. $D_{\infty h}$ has three symmetry subgroups, and they determine three quantum numbers.

The two-dimensional rotation about the charge axis corresponds to the quantum angular number, projected in the unit vector of the charge axis $\Lambda = |\mathbf{J}_g \cdot \hat{e}_z|$. The capital Greek letters $\Sigma, \Pi, \Delta, \Phi, \Gamma \ldots$ indicate as usual states with $\Lambda = 0, 1, 2, 3, 4 \ldots$, respectively. The notation is reminiscent of the $s, p, d \cdots$ waves in atomic physics. In the case of two-dimensional rotations, there are only two projections, $\mathbf{J}_g \cdot \hat{e}_z = \pm\Lambda$.

The permutation of the quark and the antiquark static charges is equivalent to a combined operation of charge conjugation and spatial inversion about the origin. Its eigenvalue is denoted by η_{CP}. States with $\eta_{\mathrm{CP}} = 1(-1)$ are denoted by the subscripts g (u), short notation for *gerade* (*ungerade*).

Moreover, there is a third quantum number, different from the phase corresponding to a two-dimensional p wave. Due to the planar, and not three-dimensional, angular momentum, there is an additional label for the s wave Σ states only. Σ states, which are even (odd) under the reflection about a plane containing the molecular axis, are denoted by a superscript $+(-)$.

With these quantum numbers, the energy levels of the flux tubes are labeled as $\Sigma_g^+, \Sigma_g^-, \Sigma_u^+, \Sigma_u^-, \Pi_u, \Pi_g, \Delta_g, \Delta_u \cdots$ The states we opt to study are most symmetric system ones, corresponding to the Σ_g^+ spectrum. This is the spectrum where up to two levels have so far been reported in the lattice QCD simulations literature [36,37]. For the other spectra, only the ground-state level has been reported in the literature [32–38]. In principle, the Σ_g^+ is the most amenable for a first study of very excited states.

In Sec. II, we thus detail the different state of the art lattice QCD techniques adequate to study the excited spectrum of the gluonic flux tubes [32–37] produced by a static quark-antiquark pair. Working with pure gauge SU(3) fields discretized in a lattice, we utilize Wilson loops with a large basis of gluonic spacelike Wilson lines to include different excitations of the quark-antiquark flux tube. Moreover, we apply different smearing techniques, an improved action, and an anisotropic lattice to improve the signal over noise ratio. We combine our operators to block diagonalize our basis the angular momentum and parity quantum numbers of the $D_{\infty h}$ point group and project on Σ_g^+ states. We numerically solve the correlation matrix via the generalized eigenvalue problem and compute the corresponding effective masses. We also discuss our computational efficiency. The number of gluonic operators combined with the space points where we compute the flux tube densities turn out to be very large, and we resort to computations in graphics processing units (GPUs) and to CUDA codes.

In Sec. III we show, for the excited levels where the signal is clear, the results of our computations for the spectrum. We evaluate how the different techniques

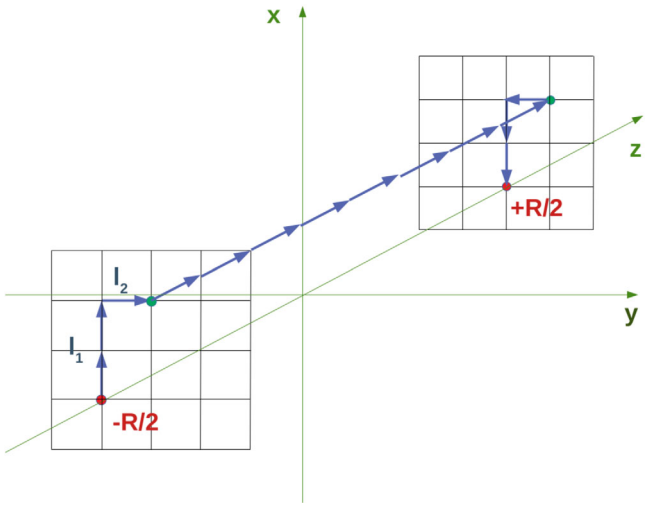

FIG. 1. Example of a Wilson spacial path from the antiquark to the quark, to be used as one of the components of the flux tube operator $O(2,1)$. The z axis is the charges axis, and xy is the perpendicular spatial plane.

improve the results. Finally, in Sec. IV, we analyze our results for the first excitations of the flux tube and search for signals of novel phenomena beyond the Nambu-Goto string model; in Sec. V, we conclude our work.

II. LATTICE QCD FRAMEWORK TO COMPUTE THE Σ_g^+ FLUX TUBES

We discuss our strategy to compute as many radially excited states as we can for the Σ_g^+ flux tubes. We consider a large basis of operators, use the standard action and an improved one, apply different smearing techniques in the configurations, and use different lattices with space-time anisotropy.

A. Our operator basis for the Σ_g^+ excited states

Our gauge invariant operators are a collection of Wilson loops, a closed path of Wilson lines. Since we have static charges, our temporal Wilson lines are quite simple; they are straight lines.

We want our spatial operators to have the same symmetry as the flux tubes we are studying. Moreover, since we are using a correlation matrix, we want any linear combination of our operators to also have the same symmetry. Otherwise, we could be producing unwanted states. The symmetry is provided by the spacial Wilson lines, who close the Wilson loop and make it gauge invariant.

In the study of the flux tubes, we utilize a basis of spacial Wilson line operators, with the necessary and sufficient operators to produce the Σ_g^+ spectrum and avoid producing the other spectra. As usual, we choose our frame such that the charge axis is the z axis, and the origin is set at the midpoint between the quark and the antiquark, with distance R. The x and y axis are in the two perpendicular directions, as illustrated in Fig. 1.

We first must choose a basis of operators, consisting of a linear combination of a set of spatial Wilson curves connecting the two static charges, with the same symmetries as those of Σ_g^+. Each curve we consider first departs from the antiquark charge in the xy plane perpendicular to the charge. In Fig. 2, we show different such curves. Then, the path of the operator is continued with a straight Wilson line in the z direction, and finally, it is completed with an opposite curve in the x, y plane to join the quark charge. The operators must be invariant for rotations of angles multiple of $\pi/2$ around the charge axis; thus, we must have a sum of n_{op} different paths in order to achieve this invariance.

In Fig. 2, we show the denomination of the operator $O(l_1, l_2)$, the distance l between the straight section of the Wilson line and the charge axis, and the number of terms n_{op} in the operator to make it symmetric. For instance, the first operator $O(0,0)$ is the simple straight Wilson line directly connecting the two charges; it has $l = 0$ and just $n_{\mathrm{op}} = 1$ term. The next operators are deformations of the

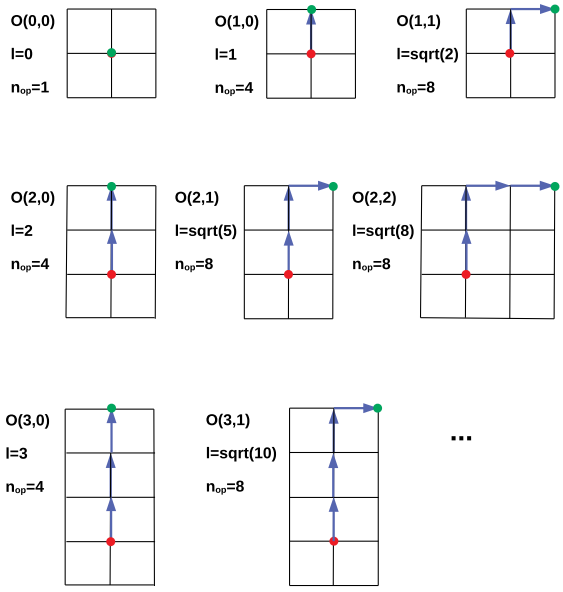

FIG. 2. Detail of the section, in the xy plane perpendicular to the charge z axis, of Wilson spacial paths from the antiquark to the quark. These examples correspond to a suboperator used in the gauge field operators $O(l_1, l_2)$. The full operator has the symmetric sum of the corresponding set of n_{op} operators, all at the same distance $l = \sqrt{{l_1}^2 + {l_2}^2}$ from the charge z axis.

straight Wilson line. Then, the operator $O(1,0)$ is a staple with $l = 1$, but we need to add $N_{\mathrm{op}} = 4$ of these staples in different directions to have an invariant operator for rotations of angles multiple of $\pi/2$ around the charge axis. The subsequent operator $O(1,1)$ has its straight z direction line at distance $l = \sqrt{2}$ from the charge axis, but for it to be invariant for the two-dimensional rotation around the charge axis and invariant for the parity inversion about the median point, we need to have a sum of all $n_{\mathrm{op}} = 8$ of these possible Wilson curves to get a fully symmetric operator. Continuing along this way, we can construct an infinite tower of symmetric operators.

Obviously, we must truncate the set of operators up to some distance l_{max} of the order of half the spatial length of the lattice since our lattice has periodic boundary conditions. Ideally, we should have l_{max} larger than the finite width of the flux tubes.

However, in contradistinction with the continuum, in a cubic lattice, there is a mixing between particular different angular momenta Λ operators. Let us consider, for instance, the operators such as the $O(l_1, l_2)$, which are a linear combination of suboperators pointing in four directions separated by right or flat angles of $0, \pi/2, \pi, 3\pi/2$. An operator with planar angular momentum Λ must have [42], for each of its spatial links as described, for instance, in Fig. 2, the phase,

$$\exp(\pm 2\pi i \Lambda \varphi), \tag{1}$$

where φ is the azimuthal angle corresponding to the respective spatial link. In the four directions of our operator, any angular momentum multiple of four,

$$\Lambda = 0, 4, 8 \cdots, \tag{2}$$

has the same phase in all four directions. Thus, we must be aware of this problem and do our best to mitigate it. This is further complicated by the phenomenology of flux tubes; in the Nambu-Goto model, there is as well a degeneracy between the excited states of these operators.

In particular, we must be careful to prevent the combinations of the symmetric operators $O(l_1, l_2)$ to generate other symmetries. These operators are discrete; they include, in general, Wilson lines in four to eight directions, and all these directions have the same phase. Having the same phase in all directions is necessary for a fully symmetric Σ_g^+ operator. However, when combining different operators with different directions, a nonsymmetric operator may be generated. For instance, $O(1,0)$, which azimuthal directions in the xy plane are $\varphi = 0, \pi/2, \pi, 3\pi/2$, and $O(1,1)$, which azimuthal directions in the xy plane are $\varphi = \pi/4, 3\pi/4, 5\pi/4, 7\pi/4$, may be combined with an opposite phase, for instance, $O(1,0) - O(1,1)$ in the case they are both properly normalized, which would correspond to a Γ_g state.

Indeed, if these $O(l_1, l_2)$ operators are all included in a correlation matrix, its diagonalization will pick up not only Σ_g^+ states but also states with large angular momentum $\Lambda = 4$ about the charge axis. We explicitly verified that, when using a wider basis of operators $O(l_1, l_2)$, we would get more energy levels, some of them nearly degenerate, than expected. Besides, the signal of the excited potentials would be less clear.

We thus restrict our basis of operators to avoid as much as possible states other than Σ_g^+. We only consider operators whose set of Wilson curves have the same directions. It is convenient to use the operators on the directions x and y of the lattice axes. For completeness, we show in Fig. 3 the four suboperators, spatial Wilson line paths from the antiquark to the quark, used to construct the gauge field operators,

$$O(l,0) = \frac{1}{\sqrt{4}}(L_x + L_{\bar{x}} + L_y + L_{\bar{y}}), \tag{3}$$

at Euclidean time t_0. The inverse Wilson lines are used for the operators at time t.

Our basis to construct the correlation matrix consists of the operators of type $O(l,0)$ only, but considering several different l. It is interesting that using a smaller operator basis and less dense in the space of the flux tube lead to clearer results for the spectrum of excited states as we found out in our computation.

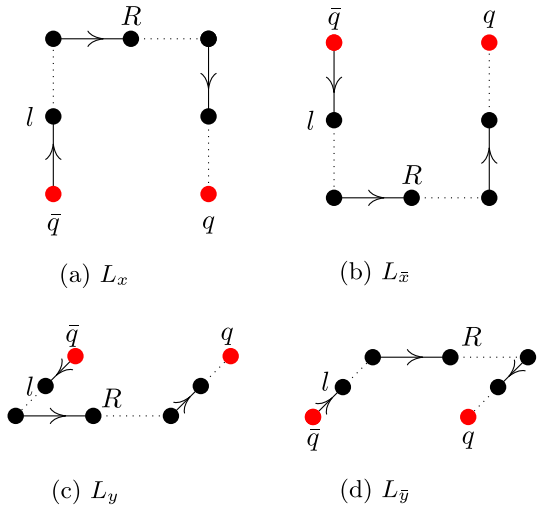

FIG. 3. The sub-operators used to construct the Wilson line $O(l,0)$ in Eq. (3).

B. Solving the GEVP for the correlation matrix to compute the excited spectra

We utilize the correlation matrix $\langle \mathcal{C}_{kl}(t) \rangle$ to compute the energy levels of the excited states, as done previously in the literature [43–46]. Now the subindices k and l stand for the spacial operators in the operator basis defined in Sec. II A, denoted O_k. The spacial operators, defined in Figs. 1–3, are connected by temporal Wilson lines L,

$$\mathcal{C}_{kl}(t) = \langle O_k(-\mathbf{R}/2, \mathbf{R}/2, 0) L(\mathbf{R}/2, 0, t) O_l^\dagger(-\mathbf{R}/2, \mathbf{R}/2, t) L^\dagger(-\mathbf{R}/2, 0, t) \rangle. \tag{4}$$

Notice each matrix element corresponds to an evolution operator in Euclidean space, where all energy levels E_i contribute, with coefficients depending on how close the operator is to the actual physical states, with the Euclidean damping factor $\exp(-E_i t)$.

The first step to compute the energy levels, is to diagonalize the generalized eigenvalue problem for the correlation matrix,

$$\mathcal{C}(t) v_n(t, t_0) = \lambda_n(t, t_0) \mathcal{C}(t_0) v_n(t_0), \tag{5}$$

for each time extent t of the Wilson loop and get a set of time dependent eigenvalues $\lambda_i(t)$. With the time dependence, we study the effective mass plot,

$$E_i \simeq \log \frac{\lambda_i(t)}{\lambda_i(t+1)}, \tag{6}$$

and search for clear plateaux consistent with a constant energy E_i in intervals $t \in [t_{i\text{ini}}, t_{i\text{fin}}]$ between the initial and

final time of the plateau. We have the option of choosing the initial time, and we choose $t_0 = 0$ because it produces the clearest results. Moreover, the results with $t_0 = 0$ are compatible with the ones obtained with other small values of t_0.

The different energies levels E_i should correspond to the ground state and excited states of the flux tube. If our operator basis is good enough, then E_0 is extremely close to the ground-state energy, E_1 is very close to the first excited state, etc.

Moreover, with the diagonalization, we also obtain the eigenvector operators [46] corresponding to the ground state, first excitation, etc. We get a linear combination of our initial operators,

$$\begin{aligned}\tilde{O}_0 &= c_{01}O_1 + c_{02}O_2 + \cdots \\ \tilde{O}_1 &= c_{11}O_1 + c_{12}O_2 + \cdots \\ &\cdots\end{aligned} \tag{7}$$

Notice this result must be interpreted with a grain of salt. The eigenvector operators $\tilde{O}_i$ do not exactly correspond to the respective state as in quantum mechanics, but they get the clearest possible signal to noise ratio, among our operator basis.

The eigenvector operators $\tilde{O}_i$ and the respective correlation matrix can be used in the same time interval $t \in [t_{i\text{ini}}, t_{i\text{fin}}]$, ideal for the effective mass plateaux of the energy spectrum.

The number of gluonic operators turns out to be large, requiring a large computer power. We thus write all our codes in CUDA and run them in computer servers with NVIDIA GPUs. Due to the GPU limited memory, this requires an intensive use of atomic memory operations. For instance, to compute a 13×13 correlation matrix, per configuration, our CUDA code takes approximately 380s for a lattice volume of $24^3 \times 96$ using a GeForce RTX 2080 Ti with 7.5 cc.

C. Gluon actions and configuration ensembles

We compute our results using six different ensembles, defined in Table I.

We use the anisotropic Wilson action [1] computed with plaquettes,

$$S_{\text{Wilson}} = \beta\left(\frac{1}{\xi}\sum_{x,s>s'} W_{s,s'} + \xi\sum_{x,s} W_{s,t}\right), \tag{8}$$

where $W_c = \sum_c \frac{1}{3}\text{ReTr}(1 - P_c)$, where s, s' runs over spatial links in different positive directions, $P_{s,s'}$ denotes the spatial plaquette, $P_{s,t}$ the spatial-temporal plaquettes, and ξ is the (unrenormalized) anisotropy.

Moreover, to improve our signal, we also resort to the improved anisotropic action S_{II} developed in Ref. [47],

$$\begin{aligned}S_{\text{II}} = \beta\Bigg(&\frac{1}{\xi}\sum_{x,s>s'}\left[\frac{5W_{s,s'}}{3u_s^4} - \frac{W_{ss,s'} + W_{s's',s}}{12u_s^6}\right] \\ &+ \xi\sum_{x,s}\left[\frac{4W_{s,t}}{3u_s^2u_t^2} - \frac{W_{ss,t}}{12u_s^4u_t^2}\right]\Bigg),\end{aligned} \tag{9}$$

with $u_s = \langle\frac{1}{3}\text{Re Tr}P_{ss}\rangle^{1/4}$, $u_t = 1$. $W_{ss,s'}$, and $W_{ss,t}$, instead of plaquettes, include 2×1 rectangles.

So far, the results with more excited states shown in the literature, two states [36,37] and up to three in an unpublished work [48], have been obtained with this action.

We generate five different ensembles of configurations, with the parameters defined of Table I.

The anisotropy is used in order to have a smaller temporal lattice spacing a_t. This enables a better estimation on the extraction of excited states as well as a more precise result since we have more time slices for the same time intervals.

Notice an anisotropic action enables us to use larger distances with the same number of spatial lattice points. However, in order to have a good spatial resolution, it is then convenient to use an improved action, and S_{II} uses plaquettes extended up to 2×1 rectangular shapes. S_{II} is specially designed to eliminate spurious high-energy states from the gluon spectrum.

Moreover, in order to improve the signal over noise ratio, for the Wilson ensemble, we use the multihit technique in the temporal Wilson lines and the APE smearing in the

TABLE I. Our ensembles, for the isotropic Wilson action and the improved anisotropic S_{II} action. ξ is the bare anisotropy in the Lagrangian, and ξ_R is the renormalized anisotropy. The renormalized anisotropy and the lattice spacings are computed with the prescription of Sec. II D.

Ensemble	Action	Operators	β	Volume	u_s	u_t	ξ	ξ_R	$a_s\sqrt{\sigma}$	$a_t\sqrt{\sigma}$	No. of configs
O_1	Wilson	11 $O(l_1, l_2)$	6.2	$24^3 \times 48$	⋯	⋯	1	1	0.1610	0.1610	1180
O_2	Wilson	11 $O(l_1, l_2)$	5.9	$24^3 \times 48$	⋯	⋯	2	2.1737(4)	0.3088(4)	0.1421(2)	2630
W_1	Wilson	13 $O(l, 0)$	6.2	$24^3 \times 48$	⋯	⋯	1	1	0.1610	0.1610	2500
W_2	Wilson	13 $O(l, 0)$	5.9	$24^3 \times 48$	⋯	⋯	2	2.1737(4)	0.3093(2)	0.1423(1)	2170
W_4	Wilson	13 $O(l, 0)$	5.6	$24^3 \times 96$	⋯	⋯	4	4.5459(9)	0.4986(4)	0.1097(1)	3475
S_4	S_{II}	13 $O(l, 0)$	4.0	$24^3 \times 96$	0.82006	1.0	4	3.6266(32)	0.3043(3)	0.0839(1)	3575

spatial Wilson lines [14]. The multihit technique [49,50] replaces each temporal link by its thermal average,

$$U_4 \to \bar{U}_4 = \frac{\int dU_4 U_4 e^{\beta \mathrm{Tr}[U_4 F^\dagger]}}{\int dU_4 e^{\beta \mathrm{Tr}[U_4 F^\dagger]}}. \tag{10}$$

Here, it is not possible to utilize the extended multihit technique as defined in Ref. [14], because our operators in the spatial Wilson line have a broader structure. In particular, we use multihit with 100 iterations in time followed by APE smearing [51] with $\alpha = 0.4$ and 20 iterations for the Wilson action without anisotropy. For the S_{II} ensemble and for the Wilson ensembles with anisotropy, we use multihit with 100 iterations in time followed by Stout smearing [52] in space with $\alpha = 0.15$ and 20 iterations.

It turns out it is more economical, using GPUs, to perform all our computations on the fly, rather than saving configurations. In general, we first generate a configuration, then apply smearing, then compute the correlation matrix with our full operator basis. What we save to a disk is the correlation matrix. Since we generate the computations on the fly, we also list the ensemble Table I, the sets of operators used. Notice we may as well turn off smearing, to check the importance of smearing, and we study the results of ensembles W_1, W_2, W_4, and S_4 with and without smearing.

In what concerns the efficiency of our codes, for instance, using a lattice volume of $24^3 \times 96$ and the Wilson action, it takes 5s to generate a new configuration. To decorrelate the configurations, we run 50 iterations between the used configurations. Each iteration is composed by four heat bath steps followed by seven overrelaxation steps. It takes 0.8s for 100 iterations of multihit and 0.014s for 20 steps of Stout smearing in space.

D. Computing the lattice spacing and the renormalized anisotropy

In the case of isotropic actions, there is only one independent scale, arising from dimensional transmutation, since the action is conformal invariant. The physical scale is the string tension σ present in the linear term of the quark-antiquark potential. From its value, we determine the lattice spacing a. In the case of anisotropic actions, we have two different lattice spacings: the spatial a_s and the temporal a_t.

To set the scale of the lattice spacing a of the isotropic Wilson action (with $\xi = 1$) in physical units, corresponding to the ensemble W_1, we use the equations fitted in SU(3) pure gauge lattice QCD by Ref. [53],

$$(a\sqrt{\sigma})(g) = f(g^2)[1 + b_1 \hat{a}(g)^2 + b_2 \hat{a}(g)^4 + b_3 \hat{a}(g)^6]/b_0, \tag{11}$$

where g is the coupling constant of the Wilson action, and [53] the parameters are $b_0 = 0.01364$, $b_1 = 0.2731$, $b_2 = -0.01545$, and $b_3 = 0.01975$, valid in the region $5.6 \le \beta \le 6.5$,

$$\hat{a}(g) = \frac{f(g^2)}{f(g^2(\beta = 6.0))}, \tag{12}$$

$$f(g^2) = (b_0 g^2)^{-\frac{b_1}{2b_0^2}} \exp\left(-\frac{1}{2b_0 g^2}\right), \tag{13}$$

and

$$b_0 = \frac{11}{(4\pi)^2}, \qquad b_1 = \frac{102}{(4\pi)^4}. \tag{14}$$

As for anisotropic actions, the renormalized anisotropy $\xi_R = a_s/a_t$ can be determined as a function of the bare anisotropy ξ. The ground-state potential is computed with the Wilson loop, two different directions for the time direction, either the usual direction four, now anisotropic, or using one of the isotropic distances, say three. Comparing the short distance potential with both time directions, which is well determined without any smearing and is fitted with a simple function, the ratio a_s/a_t is determined.

For the pure gauge SU(3) anisotropic Wilson action, ensembles W_2 and W_4, Refs. [54,55] fit the parametrization,

$$\xi_R = (1 + \eta(\xi) g^2)\xi, \tag{15}$$

corresponding to the series,

$$Z(g^2, \xi) = \xi_R/\xi = 1 + \eta(\xi) g^2 + \mathcal{O}(g^4), \tag{16}$$

where,

$$g^2 = \frac{6}{\beta}$$
$$\eta(\xi) = 0.1687(2) - 0.16397(4)/\xi - 0.005245(2)/\xi^2. \tag{17}$$

For the S_{II} action, ensemble S_4, we have similar equations from Refs. [54,55], the only difference is in the parameters of

$$\eta(\xi_0) = 0.0955(4) - 0.0702(16)/\xi_0 - 0.0399(14)/\xi_0^2, \tag{18}$$

with $\xi_0 = \xi u_s/u_t$ and $\xi_R = (1 + \eta(\xi_0) g^2)\xi_0$. We explicitly checked these formulas comparing them with the values used in Ref. [56]. In general, both values for ξ_R are compatible within error bars; only in one case the difference is slightly larger than the error bar.

Once the physical anisotropy ratio ξ_R is determined, we determine the physical scale from the string tension. We fit

the data for the ground-state potential at large interquark distance R with the linear plus constant ansatz $c_0 + c_1 R$. We did not find any improvement in the results fitting the data with the ansatz $c_0 + c_1 r + c_2/r$. We utilize smearing to be able to fit the large distance potential. The linear term is obtained from fitting the difference for different distances R of the ground-state potential,

$$c_1 = E_0(R+1) - E_0(R), \tag{19}$$

with a plateau. The linear term depends on the spatial lattice spacing a_s, the temporal lattice spacing a_t, and the string tension σ as

$$c_1 = a_s a_t \sigma. \tag{20}$$

Therefore,

$$a_s\sqrt{\sigma} = \sqrt{c_1 \xi_R}, \tag{21}$$

$$a_t\sqrt{\sigma} = \sqrt{c_1/\xi_R}. \tag{22}$$

Note that, using the above formulas, all the results presented in this work are in units of $\sqrt{\sigma}$ for the potentials and in units of $1/\sqrt{\sigma}$ for the distances. This is the standard two step technique to determine the scales of our lattice.

Besides, there is another option to fit both lattice spacings a_s and a_t in one step, when we fit the whole excited flux tube spectrum. This will be discussed in Sec. IV when we will analyze the spectrum.

III. IMPROVED RESULTS FOR THE Σ_g^+ SPECTRUM

Extracting very excited states requires using different state of the art techniques. We first show the results of the different techniques we check to improve the signal over noise ratio. Then, we show our best results.

A. Comparing the use of several $O(l,0)$ operators with and without smearing of the gauge links

Here, we are interested in checking the effect of using a large basis of operators. If this improves the results, it can be used together with other techniques. Notice, in general, in the literature, smearing is mandatory to improve the results, already for the ground-state quark-antiquark flux tube. We thus compare the effect of using a large basis of operators to using smearing.

In Fig. 4, we compare the ground-state potential for different ensembles, using just one operator (the standard Wilson loop with $O(0,0)$) or 13 sets of operators of the type $O(l,0)$ up to $l = 12$. It turns out the use of 13 operators improves the ground-state signal, but to have the best signal for a distance large enough to be physically interesting, we need smearing. According to the plots,

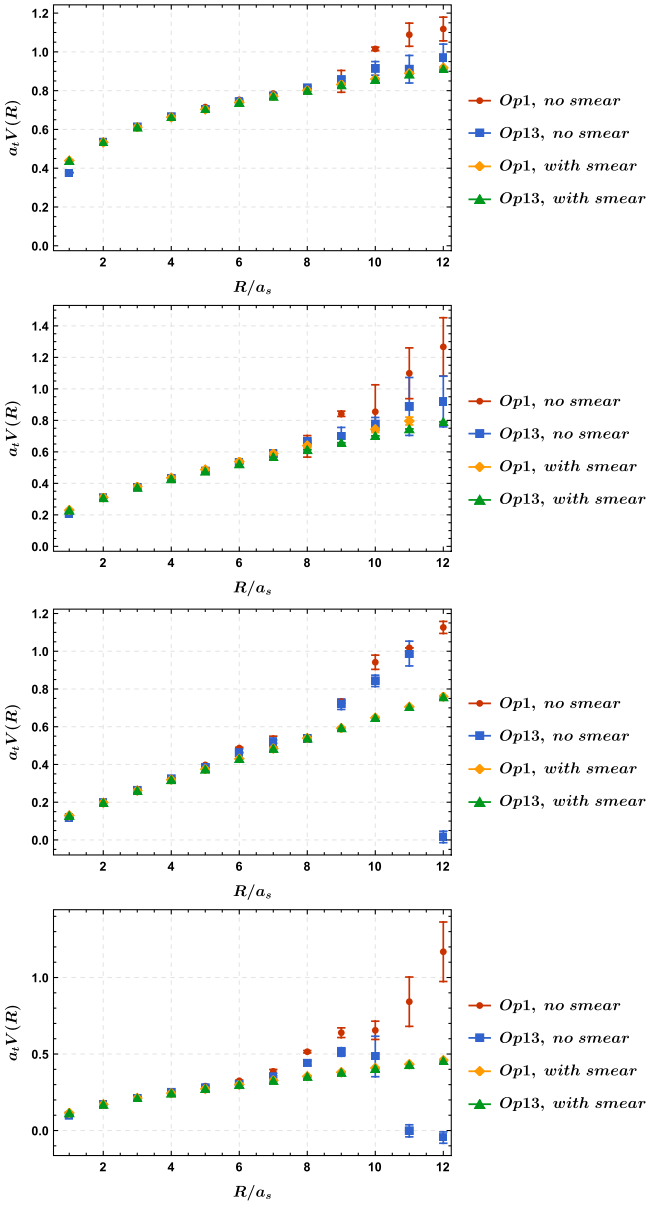

FIG. 4. Comparing results with and without a basis of operators, with and without smearing. Results for the ground state only, from top to bottom, respectively, with ensembles W_1, W_2, W_4, and S_4.

smearing maintains the results unchanged for $R > 1a_s$; in particular, the string tension error bar is reduced with smearing, but it remains consistent with the string tension with no smearing.

In Fig. 5, we use the 13 operators to search for at least one excited state, and we compare the results without and with smearing. We also include the Nambu-Goto spectrum in dashed lines to guide the eye. Indeed, the operators are necessary to get the excited sates, but in most cases, smearing is necessary as well and produces similar results to Nambu-Goto. Only in ensemble W_4, the results for the smaller distances $R < 4a_s$ can be obtained without any

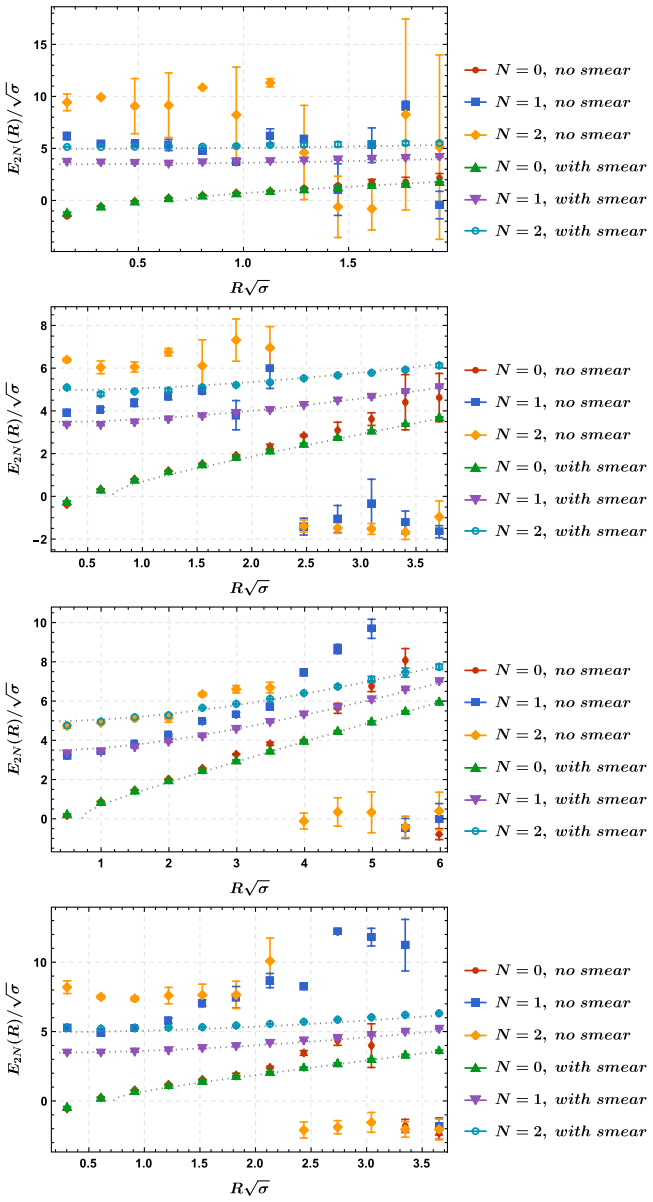

FIG. 5. Comparing results with and without smearing, using the 13 operators $O(l,0)$. To guide the eye, the Nambu-Goto model spectrum is shown in dashed lines. Results for the ground state and first two states, from top to bottom, respectively, with ensembles W_1, W_2, W_4, and S_4.

smearing for the first two excited states. Having an excited state with no smearing, similar to the smearing ones and to Nambu-Goto, confirms that smearing is not distorting our spectrum. This W_4 result also shows that an anisotropic action may be more effective to study excited states.

B. Degeneracies with $O(l_1,l_2)$ operators

We now study the results obtained with a more complete set of operators, using the ensembles O_1 and O_2 of Table I. In these simulations, we include all 11 possible operators $O(l_1,l_2)$ with $l < 4.5$, corresponding to the operators with $l_1 l_2 = 0,0;1,0;2,0;3,0;4,0;1,1;2,1;3,1;2,2;3,2;3,3$. As discussed in Sec. II A, this may produce states with different symmetries from Σ_g^+. For instance, a phase difference between operators $O(l,0)$ and operators $O(l_1,l_2)$ may be selected by the GEVP, and this could produce operators with an angular momentum four, of symmetry Γ_g^+.

This is verified in Fig. 6, where we find more states than in Fig. 7, with just the sets of operators $O(l,0)$, which are less prone to generate unwanted symmetries other than Σ_g^+. Indeed, we find approximate degeneracies among the $N = 2$, $N = 3$ states, the $N = 4$, $N = 5$, $N = 6$, and the $N = 7$, $N = 8$ states. This makes sense in the Nambu-Goto perspective where there is a principal quantum $n = 2 * n_r + l$, similar to the principal quantum number for a harmonic oscillator vibrating in a two-dimensional $x - y$ space.

From this perspective, we expect to have the degeneracies, $n = 0$, 1 state: $n_r = 0$, $n = 2$, 1 state: $n_r = 1$, $n = 4$, 3 states: $n_r = 2$ or $l = 4$, $n = 6$, 3 states: $n_r = 3$ or $n_r = 1$ and $l = 4$, $n = 8$, 5 states: $n_r = 4$ or $n_r = 2$ and $l = 4$ or $l = 8, \ldots$.

Indeed, we find in Fig. 6 nearly degenerate states $N = 2$ and $N = 3$, compatible with $n_r = 2$, $l = 0$, and $n_r = 0$, $l = 4$ states. They only differ for small distances, where possibly there are Coulomb contributions beyond the

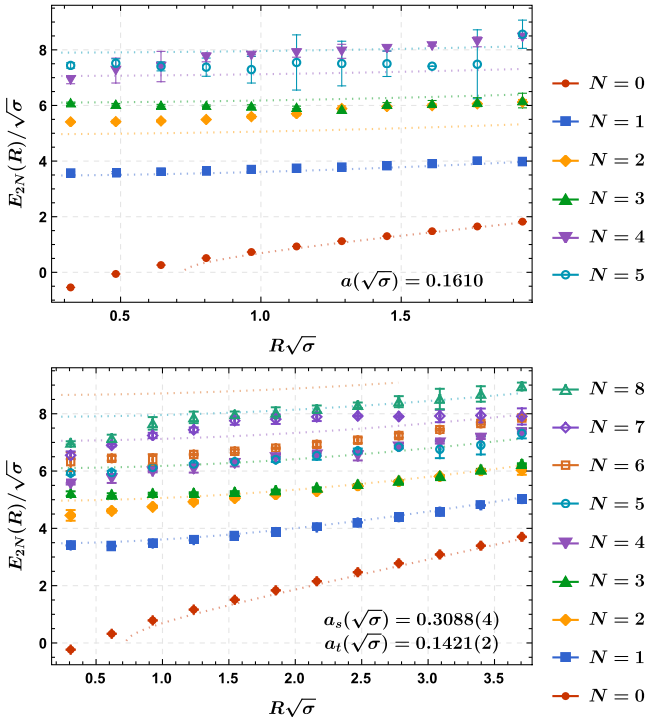

FIG. 6. Results with the enlarged basis of 11 $O(l_1,l_2)$ operators for the Wilson gauge action with APE smearing in space and multihit in time. To guide the eye, the Nambu-Goto model spectrum is shown in dashed lines. From top to bottom, respectively, with ensembles O_1 and O_2.

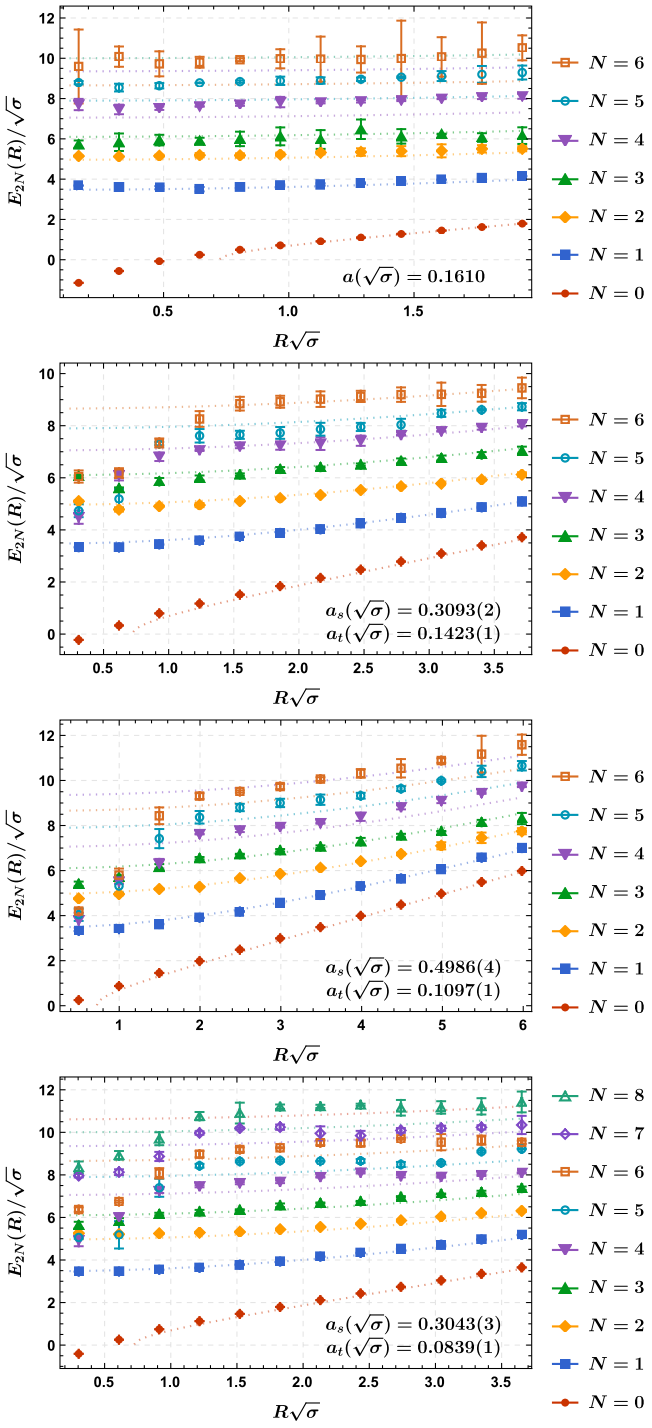

FIG. 7. Results for the full spectrum, showing only the levels obtained with good effective mass plots, from top to bottom, respectively, with ensembles W_1, W_2, W_4, and S_4. To guide the eye, the Nambu-Goto model spectrum is shown in dashed lines.

Nambu-Goto model. We also find approximate degeneracies for the higher states.

This confirms as expected that to get clearer and unambiguous Σ_g^+ signals, it is preferable to have a smaller class of operators, using only the $O(l,0)$ sets of operators.

C. Results with a basis of $O(l,0)$ operators, the Wilson action, and smearing

Using 13 sets of on-axis operators $O(l,0)$ and the Wilson action, with no anisotropy, we find already several energy levels, clearly ordered.

However, the level $N = 3$ is a bit out of the remaining patterns, with larger error bars a bit unexpectedly closer to the $N = 2$ level. This is clear in the top of Fig. 7, ensemble W_1.

The energy levels also have a similar dependence on R as in the Nambu-Goto model, constant at short distances and linear at large distances.

However, the higher levels seem to be shifted vertically when compared with the Nambu-Goto levels depicted with dotted lines.

D. Results with the Wilson action and anisotropic lattice

To get potentials at large distances, we first use the anisotropic Wilson action. The results are shown in Fig. 7 center, both for $\xi = 2$ and $\xi = 4$. Then, we are able to go not only up to large distances, but also to clearly see one more level, going up to $N = 6$.

The pattern of the separation of the levels is also more striking even than in the isotropic case.

However, the values of the higher potentials get distorted at shorter distances, perhaps because the anisotropy somehow enables the degeneracy already discussed in Secs. II A and III B to set in.

Nevertheless, the higher levels remain undistorted for $R > 4a_s$.

E. Results with the improved anisotropic action

To solve the problem at smaller distances for the anisotropic lattices, we resort to the improved action. Indeed, the short distance is improved, although it remains distorted, as seen in Fig. 7 bottom, ensemble S_4.

Nevertheless, we are able to get two more levels, $N = 7$ and 8. This is the highest level we are able to get.

We also compare the results of all actions in Fig. 8, where we study one potential level in each panel. The excited levels tend to be higher than the Nambu-Goto model.

To conclude on the different spectra, we are able to get several levels, with on-axis operators, with smearing, and with anisotropic lattices, but we should discard the first four smaller distances for the anisotropic action because the levels above $N = 2$ are distorted and tend to get degenerate.

IV. ANALYSIS OF OUR RESULTS

The simplest description of the QCD excited flux tubes—with charges in the triplet representation of SU(3)—is given by the bosonic string model, based on the Nambu-Goto action [6,7],

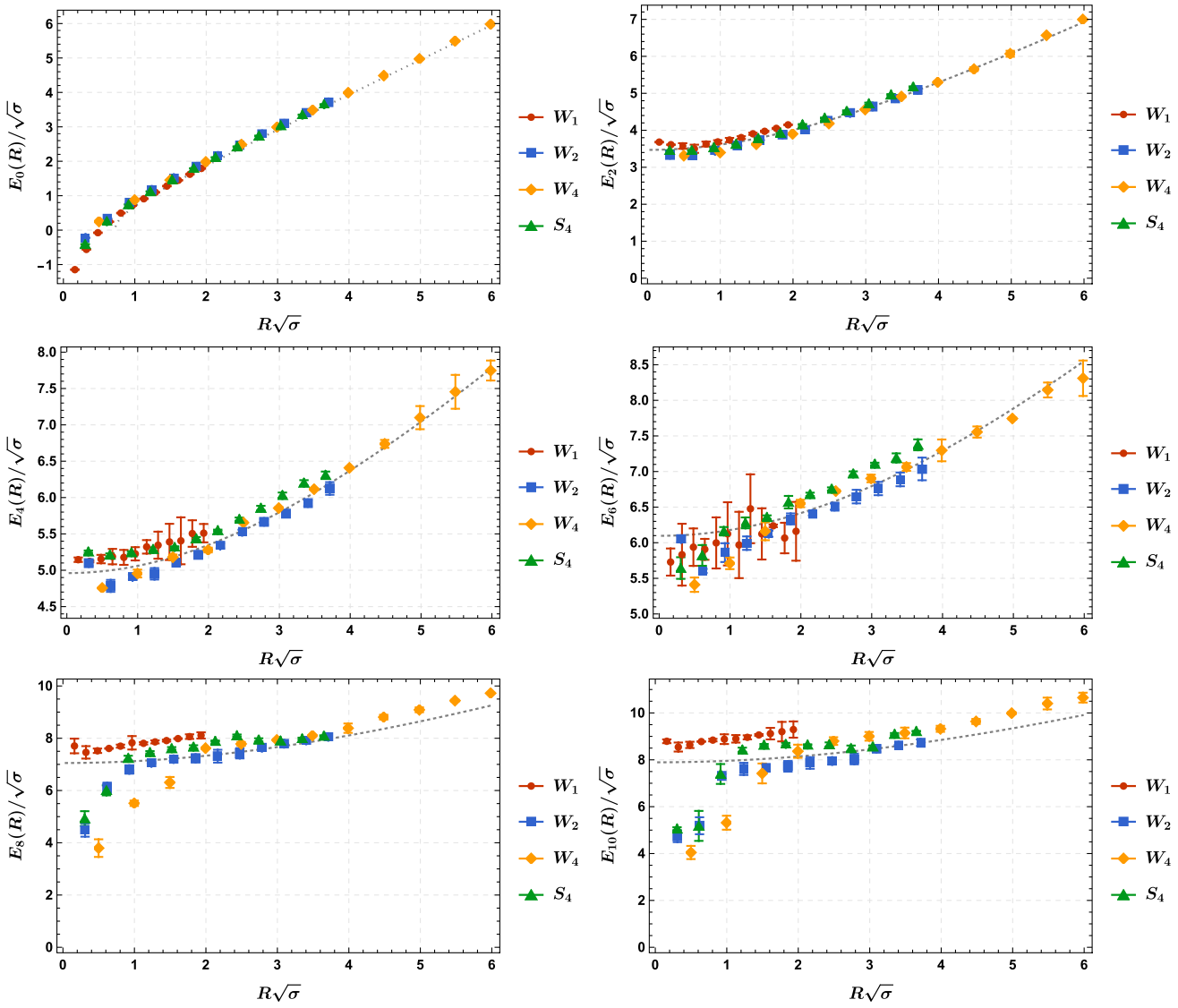

FIG. 8. Comparing the results of ensembles W_1, W_2, W_4, and S_4 for each one of the energy levels. From left to right and top to bottom, we show the ground-state potential and the first five excited states. To guide the eye, the dashed lines correspond to the corresponding level of the Nambu-Goto spectrum.

$$S = -\sigma \int d^2\Sigma, \tag{23}$$

which, for spectrum for an open string with ends fixed with Dirichlet boundary conditions is the Arvis potential [11],

$$V_n(R) = \sigma\sqrt{R^2 + \frac{2\pi}{\sigma}\left(n - \frac{D-2}{24}\right)}. \tag{24}$$

In Eq. (24), D is the dimension of the space time $D = 4$, and $n = 2n_r + l$ is the principal quantum number. In our case of Σ_g^+, $l = 0$, the only quantum number we have is $n = 2n_r$, where n_r is the order of the radial excitation. Because of this simple analytical form, we opt to fit the excited spectrum with the Arvis potential. Any deviation may indicate other phenomena, say, a constituent gluon.

Note that, for the ground state, the Arvis potential is tachyonic at small distances since the argument of the square root is negative; moreover, rotational invariance is only achieved for $D = 26$. Nevertheless, the first two terms in the $1/R$ expansion, including the Coulomb term, are more general than the Arvis potential, since they fit the $D = 3$ and $D = 4$ lattice data quite well beyond the tachyonic distance. The Coulomb term is independent of the string tension σ, and for the physical, $D = 3 + 1$ has the value $-\frac{\pi}{12}\frac{1}{R}$. This is the Lüscher term [57]. The energy spectrum of a static quark-antiquark and of its flux tube is certainly well defined (not tachionic), and this was the first evidence of flux tube vibrations found in lattice field theory.

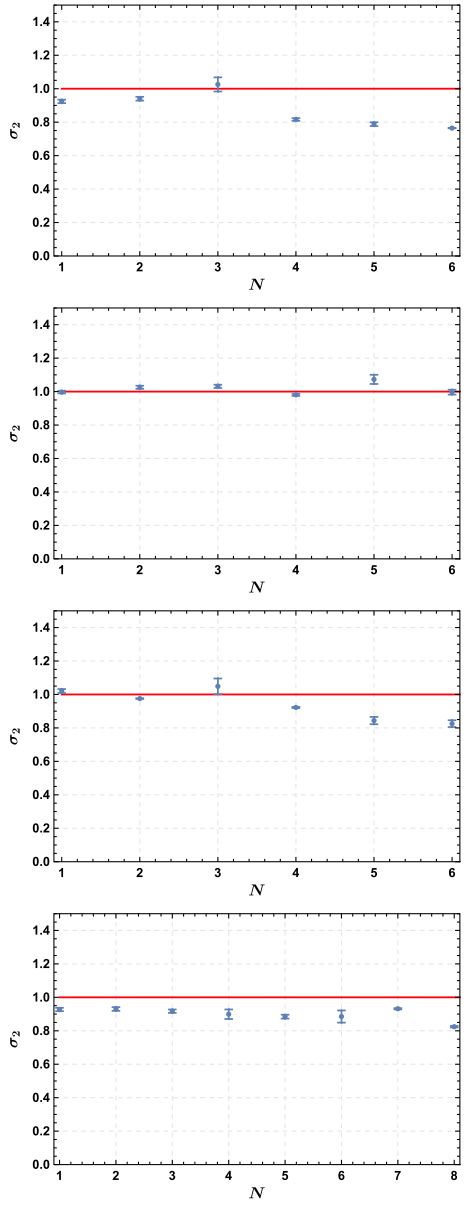

FIG. 9. Results of the fits, for the second σ_2 parameter of the modified Nambu-Goto expression, from top to bottom, respectively, with ensembles W_1, W_2, W_4, and S_4.

In what concerns the ground state, it is well known, as detailed in Sec. I, that the Nambu-Goto fails because we have no tachyon at short distances. However, the leading terms in a large distance expansion are accurate not only at long distances, but also at medium range short distances, where the tachyon is replaced by the Lüscher [57] coulombic potential,

$$V_0(R) = \sigma R - \frac{\pi}{12}\frac{1}{R} + O\left(\frac{1}{R^3}\right), \tag{25}$$

which confirms the factor $(n - \frac{D-2}{24})$ in the Arvis potential. At very short distances, the correct potential matches perturbative QCD [12].

Nevertheless, for the excited states, the intrinsic width of the flux tube [14] should become negligible compared with the quantum vibrations of the string. The Nambu-Goto model should then be adequate to analyze the potentials we compute with lattice QCD. Notice the Arvis potential produces a tower of levels,

$$\begin{aligned} V_{n_r}(R) &= \sigma\sqrt{R^2 + \frac{2\pi}{\sigma}\left(2n_r - \frac{1}{12}\right)} \\ &= \sqrt{2\pi\sigma\left(2n_r - \frac{1}{12}\right)} + O(R^2), \end{aligned} \tag{26}$$

as we observe in our lattice QCD data.

We now start analyzing our data, shown in Figs. 7 and 8, where they are compared explicitly with the Nambu-Goto model.

If we exclude the smaller four distances showing some energy degeneracy, evident in Fig. 7 in the compression of the higher levels with $N > 2$, we see no evidence for the Γ_g states, discussed in Sec. II A, degenerate with our Σ_g^+ states. Notice the degeneracy in these smaller four distances is possibly due to higher harmonics of the string vibrations. The harmonics with an even number of nodes have the

TABLE II. The different parameters σ_2/σ in the modified Nambu-Goto model fitted for all the energy levels in the different ensembles.

	σ_2/σ			
Energy level	W_1	W_2	W_4	S_4
N_1	0.9241(105)	0.9970(76)	1.0206(117)	0.9273(101)
N_2	0.9403(114)	1.0258(93)	0.9753(20)	0.9302(112)
N_3	1.0255(422)	1.0313(99)	1.0486(468)	0.9171(103)
N_4	0.8160(79)	0.9803(58)	0.9223(37)	0.8990(285)
N_5	0.7880(115)	1.0731(275)	0.8440(219)	0.8845(117)
N_6	0.7646(14)	0.9967(147)	0.8254(203)	0.8852(363)
N_7	⋯	⋯	⋯	0.9317(38)
N_8	⋯	⋯	⋯	0.8245(46)

same quantum numbers Σ_g^+ as the fundamental harmonic. Since our operators only have two nodes, at the open ends of the string, they should not have a large overlap with the higher harmonics, except at shorter distances, where the square shape of our operators may be too crude to only overlap with the fundamental harmonic. Since we are only interested in studying the radial excitations, From now on,

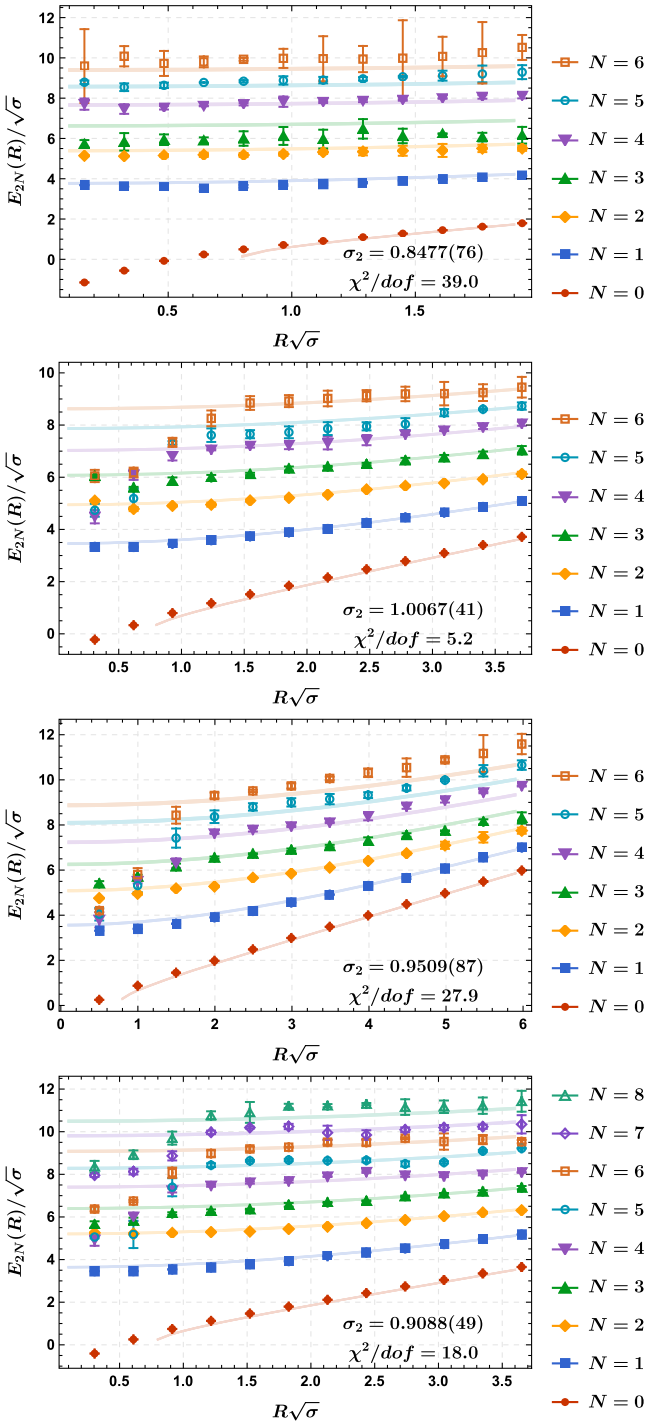

FIG. 10. Comparing our results to a fit with the modified Nambu-Gotto action, a unique σ_2 is extracted from a nonlinear multifit of all the energy levels, in the interval $[5a_s - 12a_s]$, from top to bottom, respectively, with ensembles W_1, W_2, W_4, and S_4. The width of the solid lines are equal to the error bar of our fit.

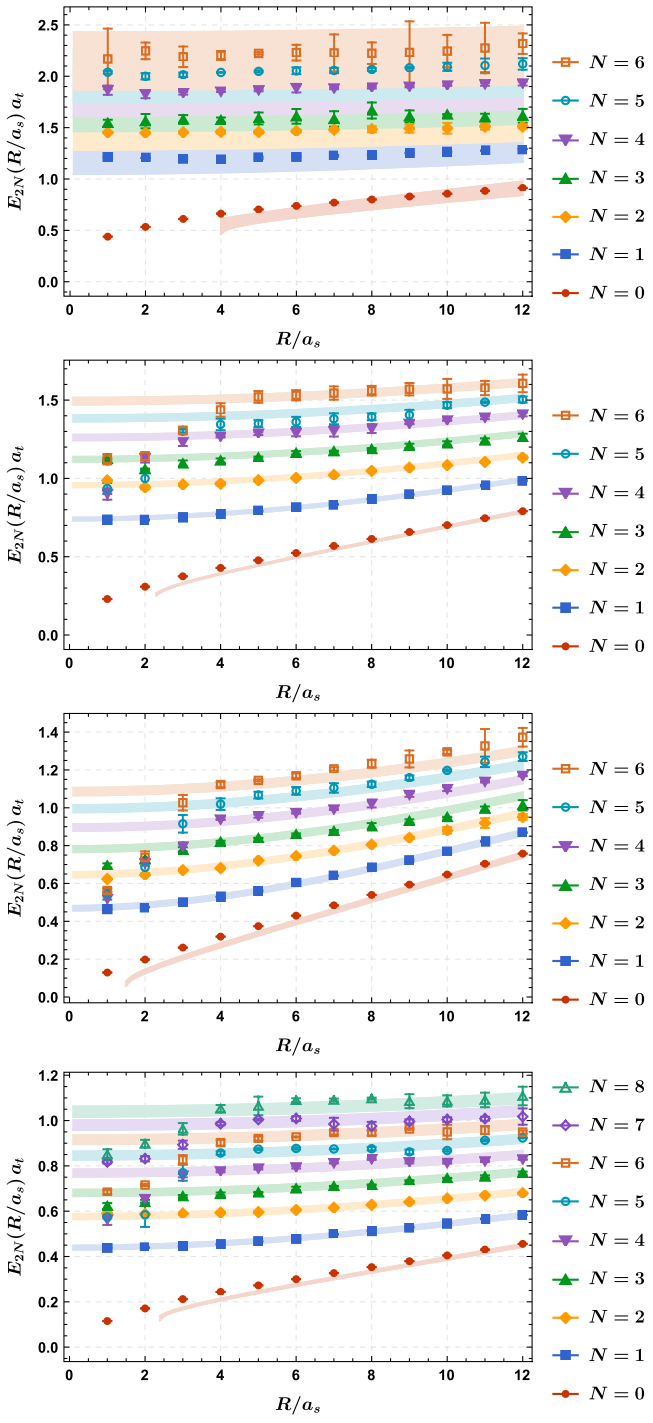

FIG. 11. Comparing our results in lattice spacing units to a fit with the modified Nambu-Gotto action the values are extracted from a nonlinear multifit of all the energy levels, in the interval $[5a_s - 12a_s]$, from top to bottom, respectively, with ensembles W_1, W_2, W_4, and S_4. The width of the solid lines are equal to the error bar of our fit. The ground state was excluded from the multifit. σ is the linear term of the ground state fitted alone.

we will exclude the four shortest distances from the fits of our data.

Moreover, we see no evidence for string breaking [58–60], noticing that with the anisotropic actions we are able to go to distances much larger than the string breaking distance. Thus, we are confident to be analyzing the pure hybrid Σ_g^+ states.

The first two excited states seem to be, in general, compatible with the Nambu-Goto model within error bars. However, the next states depart from it, apparently the energy levels are in general higher than in Nambu-Goto.

Thus, we analyze quantitatively the difference to the Nambu-Goto potential, fitting the data with an extra parameter. We multiply the constant term in the square root by an independent prefactor. The simplest way we find to do this is to change σ in to σ_2 in the denominator or the constant term depending on n_r. The modified Nambu-Goto model is

$$V_n(R) = \sigma R\sqrt{1+\frac{2\pi}{\sigma_2 R^2}\left(n-\frac{D-2}{24}\right)}. \tag{27}$$

In particular, we fit the results of Fig. 7 for each excited state separately with $E_{2N}(R)/(R\sigma)$ to $\sqrt{1+\frac{2\pi}{\sigma_2 R^2}(2N-\frac{1}{12})}$ and extract σ_2. The resulting fits of all the energy levels for the different ensembles are shown in Fig. 9 and detailed in Table II.

Besides, we also use another approach with a gobal fit of all levels. Instead of fitting each excited state separately, we perform a nonlinear multifit for all the excited states in each ensemble in Fig. 10. For each emsemble, we display the resulted σ_2 and χ^2/dof. We find that for ensembles W_1, W_4, and S_4, σ_2 is up to 10% smaller than σ (meaning that the energy levels are higher than in the Nambu-Goto model), but for W_2 and σ_2, they are similar.

Furthermore, since the results in Fig. 7 are in units of the string tension obtained from the ground-state fit, we also perform an even more global fit, fitting all parameters to the excited spectrum (and not fitting the ground state). In Fig. 11 and in Table III, we depict the nonlinear multifit for all the excited states in lattice spacing units to the equation,

$$V_n(R) = a_0 + \sigma_1 R\sqrt{1+\frac{2\pi}{\sigma_2 R^2}\left(n-\frac{D-2}{24}\right)}. \tag{28}$$

In this case, what we have to compare with the previous σ_2/σ is now $\sigma_2/\xi_R/\sigma_1$. Again, this goes down, up to 10% in ensembles W_4 and S_4, while in ensembles W_1 and W_2, this is of order of 1.

This departure of up to 10% from the Nambu-Goto model may possibly be interpreted as the string being nonhomogeneous or be interpreted with the existence of a constituent gluon in the more excited states.

V. CONCLUSIONS AND OUTLOOK

We computed the potentials for several new excitations of the pure SU(3) flux tubes produced by two static 3 and $\bar{3}$ sources, specializing in the radial excitations of the representation Σ_g^+.

We succeeded in obtaining the spectrum of several new excited flux tubes, using a large basis of operators, employing the computational techniques with GPUs of Ref. [40] (improved to be able to study field densities), and utilizing different actions with smearing and anisotropy. Previously in the literature and websites, states up to $N = 2$ have been shown, and we go up to $N = 8$.

In general, the excited states of the Σ_g^+ flux tubes are comparable to the Nambu-Goto string model with transverse modes, only depending on the string tension σ and the radial quantum number n_r.

Nevertheless, we found evidence that the Σ_g^+ flux tubes cannot be exactly modelled by the Nambu-Goto string model. A second parameter, we parametrize as a second σ_2 up to 10% smaller than σ, essentially corresponding to a larger energy splitting between levels than in the Nambu-Goto model leads to better fits. Interesting for the theoretical studies of the QCD flux tubes, this may indicate the formation of a nonhomogenous string with a lump or a constituent gluon or of an extra symmetry higher in the spectrum as referred in Sec. I.

To clarify in more detail this small tension with the Nambu-Goto model, we would need to have more computational power to be able to use larger lattices and more operators. Another direction of research is on investigating higher angular excitations of the flux tube (here we investigated radial excitations), but a new approach would

TABLE III. Fit results of the Fig. 11 extracted from a nonlinear multifit of all the energy levels, in the interval $[5a_s - 12a_s]$. The ground state was excluded from the multifit. σ is the linear term of the ground state fitted alone.

Ensemble	a_0	σ	σ_1	σ_2	σ_2/ξ_R	$\sigma_2/\xi_R/\sigma_1$	χ^2/dof
W_1	0.521(408)	⋯	0.0351(46)	0.0344(74)	0.0344(74)	0.9814(2470)	35.1
W_2	0.2363(33)	0.0440(1)	0.0468(6)	0.1039(25)	0.0478(11)	1.0205(270)	2.9
W_4	0.0564(99)	0.0547(1)	0.0583(8)	0.2400(47)	0.0528(10)	0.9062(216)	25.8
S_4	0.1203(39)	0.0255(1)	0.0279(5)	0.0923(29)	0.0255(8)	0.9116(329)	13.7

be necessary to overcome the limitations of a cubic lattice. Searching in different quantum numbers for explicit evidences of a constituent gluon [41] or of an axion [29] is also motivating. We leave this for future works.

ACKNOWLEDGMENTS

We acknowledge discussions on flux tubes and constituent gluons with our colleagues Sergey Afonin, Gunnar Bali, Daniele Binosi, Bastian Brandt, Richard Brower, Fabien Buisseret, Leonid Glozman, Alexei Kaidalov, Felipe Llanes-Estrada, Vincent Mathieu, Colin Morningstar, Lasse Müller, Fumiko Okiharu, Orlando Oliveira, Emilio Ribeiro, and Marc Wagner. We thank the support of Centro de Física e Engenharia de Materiais Avançados (Center of Physics and Engineering of Advanced Materials) under the contract for R&D Units, strategic Project No. UID/CTM/04540/2019, and the FCT project Grant No. CERN/FIS-COM/0029/2017. N. C. is supported by FCT under the Contract No. SFRH/BPD/109443/2015, and A. S. is supported by the Contract No. SFRH/PD/BD/135189/2017.

[1] K. G. Wilson, Confinement of quarks, Phys. Rev. D **10**, 2445 (1974).
[2] P. Bicudo, The large degeneracy of excited hadrons and quark models, Phys. Rev. D **76**, 094005 (2007).
[3] P. Bicudo, Gluon excitations and quark chiral symmetry in the meson spectrum: An Einbein solution to the large degeneracy problem of light mesons, Phys. Rev. D **81**, 014011 (2010).
[4] S. Godfrey and N. Isgur, Mesons in a relativized quark model with chromodynamics, Phys. Rev. D **32**, 189 (1985).
[5] N. Isgur and G. Karl, P wave baryons in the quark model, Phys. Rev. D **18** (1978) 4187.
[6] Y. Nambu, QCD and the string model, Phys. Lett. **80B**, 372 (1979).
[7] T. Goto, Relativistic quantum mechanics of one-dimensional mechanical continuum and subsidiary condition of dual resonance model, Prog. Theor. Phys. **46**, 1560 (1971).
[8] O. Aharony and E. Karzbrun, On the effective action of confining strings, J. High Energy Phys. 06 (2009) 012.
[9] F. Gliozzi, M. Pepe, and U. J. Wiese, The Width of the Confining String in Yang-Mills Theory, Phys. Rev. Lett. **104**, 232001 (2010).
[10] O. Alvarez, The static potential in string models, Phys. Rev. D **24**, 440 (1981).
[11] J. F. Arvis, The exact $q\bar{q}$ potential in Nambu string theory, Phys. Lett. **127B**, 106 (1983).
[12] F. Karbstein, A. Peters, and M. Wagner, $\Lambda_{\overline{\mathrm{MS}}}^{(n_f=2)}$ from a momentum space analysis of the quark-antiquark static potential, J. High Energy Phys. 09 (2014) 114.
[13] http://saturno.ist.utl.pt/~ptqcd (2007).
[14] N. Cardoso, M. Cardoso, and P. Bicudo, Inside the SU(3) quark-antiquark QCD flux tube: Screening versus quantum widening, Phys. Rev. D **88**, 054504 (2013).
[15] D. V. Bugg, Four sorts of meson, Phys. Rep. **397**, 257 (2004).
[16] E. Aker *et al.*, The crystal barrel spectrometer at LEAR, Nucl. Instrum. Methods Phys. Res., Sect. A **321**, 69 (1992).
[17] L. Y. Glozman, Restoration of chiral and U(1)A symmetries in excited hadrons, Phys. Rep. **444**, 1 (2007).
[18] S. S. Afonin, Light meson spectrum and classical symmetries of QCD, Eur. Phys. J. A **29**, 327 (2006).
[19] S. S. Afonin, Towards understanding spectral degeneracies in nonstrange hadrons. Part I. Mesons as hadron strings versus phenomenology, Mod. Phys. Lett. A **22**, 1359 (2007).
[20] L. Y. Glozman, C. B. Lang, and M. Schrock, Symmetries of hadrons after unbreaking the chiral symmetry, Phys. Rev. D **86**, 014507 (2012).
[21] M. Catillo and L. Y. Glozman, Baryon parity doublets and chiral spin symmetry, Phys. Rev. D **98**, 014030 (2018).
[22] C. Semay, F. Buisseret, and B. Silvestre-Brac, Towers of hybrid mesons, Phys. Rev. D **79**, 094020 (2009).
[23] E. Abreu and P. Bicudo, Glueball and hybrid mass and decay with string tension below Casimir scaling, J. Phys. G **34**, 195 (2007).
[24] F. Buisseret and C. Semay, On two- and three-body descriptions of hybrid mesons, Phys. Rev. D **74**, 114018 (2006).
[25] J. M. Cornwall, Dynamical mass generation in continuum QCD, Phys. Rev. D **26**, 1453 (1982).
[26] O. Oliveira and P. Bicudo, Running gluon mass from landau gauge lattice QCD propagator, J. Phys. G **38**, 045003 (2011).
[27] P. Bicudo, M. Cardoso, and O. Oliveira, Study of the gluon-quark-antiquark static potential in SU(3) lattice QCD, Phys. Rev. D **77**, 091504 (2008).
[28] M. Cardoso, N. Cardoso, and P. Bicudo, Lattice QCD computation of the color fields for the static hybrid quark-gluon-antiquark system, and microscopic study of the Casimir scaling, Phys. Rev. D **81**, 034504 (2010).
[29] S. Dubovsky, R. Flauger, and V. Gorbenko, Evidence from Lattice Data for a New Particle on the Worldsheet of the QCD Flux Tube, Phys. Rev. Lett. **111**, 062006 (2013).
[30] A. Athenodorou, B. Bringoltz, and M. Teper, Closed flux tubes and their string description in $D = 3 + 1$ SU(N) gauge theories, J. High Energy Phys. 02 (2011) 030.
[31] B. Lucini and M. Panero, SU(N) gauge theories at large N, Phys. Rep. **526**, 93 (2013).
[32] N. A. Campbell, A. Huntley, and C. Michael, Heavy quark potentials and hybrid mesons from SU(3) lattice gauge theory, Nucl. Phys. **B306**, 51 (1988).
[33] S. Perantonis and C. Michael, Static potentials and hybrid mesons from pure SU(3) lattice gauge theory, Nucl. Phys. **B347**, 854 (1990).

[34] P. Lacock, C. Michael, P. Boyle, and P. Rowland, Hybrid mesons from quenched QCD, Phys. Lett. B **401**, 308 (1997).
[35] P. Lacock, C. Michael, P. Boyle, and P. Rowland, Orbitally excited and hybrid mesons from the lattice, Phys. Rev. D **54**, 6997 (1996).
[36] K. J. Juge, J. Kuti, and C. J. Morningstar, Ab Initio Study of Hybrid Anti-b g b Mesons, Phys. Rev. Lett. **82**, 4400 (1999).
[37] K. J. Juge, J. Kuti, and C. Morningstar, Fine Structure of the QCD String Spectrum, Phys. Rev. Lett. **90**, 161601 (2003).
[38] C. Reisinger, S. Capitani, O. Philipsen, and M. Wagner, Computation of hybrid static potentials in SU(3) lattice gauge theory, EPJ Web Conf. **175**, 05012 (2018).
[39] L. Müller and M. Wagner, Different modes of elliptic and triangular flow in ultrarelativistic PbPb collisions from HYDJET model, Acta Phys. Pol. B Proc. Suppl. **11**, 551 (2018).
[40] P. Bicudo, N. Cardoso, and M. Cardoso, Color field densities of the quark-antiquark excited flux tubes in SU(3) lattice QCD, Phys. Rev. D **98**, 114507 (2018).
[41] L. Müller, O. Philipsen, C. Reisinger, and M. Wagner, Hybrid static potential flux tubes from SU(2) and SU(3) lattice gauge theory, Phys. Rev. D **100**, 054503 (2019).
[42] S. Capitani, O. Philipsen, C. Reisinger, C. Riehl, and M. Wagner, Precision computation of hybrid static potentials in SU(3) lattice gauge theory, Phys. Rev. D **99**, 034502 (2019).
[43] B. Blossier, M. Della Morte, G. von Hippel, T. Mendes, and R. Sommer, On the generalized eigenvalue method for energies and matrix elements in lattice field theory, J. High Energy Phys. 04 (2009) 094.
[44] J. J. Dudek, R. G. Edwards, M. J. Peardon, D. G. Richards, and C. E. Thomas, Highly Excited and Exotic Meson Spectrum from Dynamical Lattice QCD, Phys. Rev. Lett. **103**, 262001 (2009).
[45] J. J. Dudek, R. G. Edwards, M. J. Peardon, D. G. Richards, and C. E. Thomas, Toward the excited meson spectrum of dynamical QCD, Phys. Rev. D **82**, 034508 (2010).
[46] P. Bicudo, A. Peters, S. Velten, and M. Wagner, Importance of meson-meson and of diquark-antidiquark creation operators for a $\bar{b}\,\bar{b}\,ud$ tetraquark, Phys. Rev. D **103**, 114506 (2021).
[47] C. Morningstar, Improved gluonic actions on anisotropic lattices, Nucl. Phys. B, Proc. Suppl. **53**, 914 (1997).
[48] C. Morningstar, Excitations of the static-quark potential, su(3) in 4 dimensions, https://www.andrew.cmu.edu/user/cmorning/static_potentials/SU3_4D/B30_AR3/plots/Rplots.html.
[49] R. Brower, P. Rossi, and C.-I. Tan, The external field problem for QCD, Nucl. Phys. **B190**, 699 (1981).
[50] G. Parisi, R. Petronzio, and F. Rapuano, A measurement of the string tension near the continuum limit, Phys. Lett. **128B**, 418 (1983).
[51] M. Albanese *et al.*, Glueball masses and string tension in lattice QCD, Phys. Lett. B **192**, 163 (1987).
[52] C. Morningstar and M. J. Peardon, Analytic smearing of SU(3) link variables in lattice QCD, Phys. Rev. D **69**, 054501 (2004).
[53] R. G. Edwards, U. M. Heller, and T. R. Klassen, Accurate scale determinations for the Wilson gauge action, Nucl. Phys. **B517**, 377 (1998).
[54] I. T. Drummond, A. Hart, R. R. Horgan, and L. C. Storoni, One loop calculation of the renormalized anisotropy for improved anisotropic gluon actions on a lattice, Phys. Rev. D **66**, 094509 (2002).
[55] I. T. Drummond, A. Hart, R. R. Horgan, and L. C. Storoni, The contribution of O(alpha) radiative corrections to the renormalized anisotropy and application to general tadpole improvement schemes: Addendum to 'One loop calculation of the renormalized anisotropy for improved anisotropic gluon actions on a lattice', Phys. Rev. D **68**, 057501 (2003).
[56] Morningstar, https://www.andrew.cmu.edu/user/cmorning/static_potentials/SU3_4D/greet.html.
[57] M. Luscher, G. Munster, and P. Weisz, How thick are chromoelectric flux tubes?, Nucl. Phys. **B180**, 1 (1981).
[58] G. S. Bali, H. Neff, T. Duessel, T. Lippert, and K. Schilling, Observation of string breaking in QCD, Phys. Rev. D **71**, 114513 (2005).
[59] J. Bulava, B. Hörz, F. Knechtli, V. Koch, G. Moir, C. Morningstar, and M. Peardon, String breaking by light and strange quarks in QCD, Phys. Lett. B **793**, 493 (2019).
[60] P. Bicudo, M. Cardoso, N. Cardoso, and M. Wagner, Bottomonium resonances with $I = 0$ from lattice QCD correlation functions with static and light quarks, Phys. Rev. D **101**, 034503 (2020).